Radioimmunotherapy of Head and Neck Cancer Xenografts Using ^{131}I-Labeled Antibody L19-SIP for Selective Targeting of Tumor Vasculature

Bernard M. Tijink[1], Dario Neri[2], C. René Leemans[1], Marianne Budde[1], Ludger M. Dinkelborg[3], Marijke Stigter-van Walsum[1], Luciano Zardi[4], and Guus A.M.S. van Dongen[1]

[1]Department of Otolaryngology/Head and Neck Surgery, VU University Medical Center, Amsterdam, The Netherlands; [2]Institute of Pharmaceutical Sciences, Swiss Federal Institute of Technology, Zurich, Switzerland; [3]Research Laboratories of Schering AG, Berlin, Germany; and [4]Laboratory of Innovative Therapy, Advanced Biotechnology Center, Istuto Giannina Gaslini, Genova, Italy

The extra domain B of fibronectin (ED-B) is a marker of tumor angiogenesis. The human monoclonal antibody (mAb) L19-SIP (~80 kDa; SIP is "small immunoprotein") has been selected for targeting of ED-B. The aim of this study was to evaluate the potential of radioimmunotherapy (RIT) with L19-SIP, either alone or in combination with cetuximab, for treatment of head and neck squamous cell carcinoma (HNSCC). Combination with cetuximab was considered because this anti-EGFR (epidermal growth factor receptor) mAb has proven value for the treatment of HNSCC. **Methods:** HNSCC xenograft lines FaDu and HNX-OE were evaluated for ED-B and EGFR expression. L19-SIP was radiolabeled with 2 candidate radionuclides for RIT, ^{177}Lu and ^{131}I (or ^{125}I as substitute). The biodistribution of coinjected ^{177}Lu-L19-SIP and ^{125}I-L19-SIP was assessed in FaDu-bearing nude mice, whereas ^{131}I-L19-SIP was evaluated in both xenograft lines. After labeling with high-dose ^{131}I (623–789 MBq/mg), the maximum tolerated dose (MTD) was assessed. The efficacy of RIT with injected ^{131}I-L19-SIP, either alone or in combination with unlabeled cetuximab (1 mg 2 times a week intraperitoneally for 4 wk), was evaluated in both xenograft lines. **Results:** Xenograft lines expressed both antigens, with similar EGFR expression and the highest ED-B expression in FaDu. Radioiodinated L19-SIP performed better than ^{177}Lu-L19-SIP and was further exploited. The biodistribution of ^{131}I-L19-SIP was most favorable in FaDu-bearing mice, with tumor uptake values at 24, 48, and 72 h after injection of 8.6 ± 1.6, 5.8 ± 0.4, and 3.4 ± 0.2 %ID/g (%ID/g is percentage injected dose per gram of tissue), respectively, and ratios of tumor to normal tissues that gradually increased in time, such as for blood from 4.4 ± 1.8 at 24 h to 21.4 ± 1.7 at 72 h, after injection. RIT at the MTD level of 74 MBq caused significant tumor growth delay and improved survival in both lines. Although FaDu was most sensitive for RIT, with size reduction of all tumors, HNX-OE was most sensitive for treatment with cetuximab. The best survival and cure rates were obtained, however, when RIT and cetuximab were combined. **Conclusion:** RIT with ^{131}I-L19-SIP appeared efficacious in HNSCC xenografts. The efficacy of RIT was enhanced by combination with cetuximab, without increase of toxicity.

Key Words: radioimmunotherapy; L19-SIP; squamous cell carcinoma; ED-B; angiogenesis

J Nucl Med 2006; 47:1127–1135

Angiogenesis is one of the hallmarks of cancer and, therefore, considerable efforts have been invested in the discovery of agents that block this process. One approach aims at the neutralization of growth factors and other angiogenic mediators involved in endothelial cell migration and proliferation. The potential of this approach is best exemplified by studies aiming at the neutralization of vascular endothelial growth factor (VEGF) activity, either by capturing the growth factor itself or by blockage of its receptor (*1,2*). The neutralizing humanized anti-VEGF monoclonal antibody (mAb) bevacizumab (Avastin; Genentech) has recently been approved for use in combination with 5-fluorouracil–based chemotherapy as a first-line treatment for metastatic colorectal cancer (*3*). A potential hurdle in approaches aiming at the neutralization of one critical proangiogenic factor is that other redundant proangiogenic factors may compensate for the one that is inhibited.

Another appealing therapeutic approach is the targeted destruction of established tumor vasculature—for example, by mAbs directed against markers of angiogenesis (*1,2*). An interesting candidate target for this approach is the extra domain B (ED-B) of fibronectin (FN). FN is an extracellular matrix component that is widely expressed in a variety of normal tissues and body fluids. Different FN isoforms can be generated by alternative splicing, a process modulated by cytokines and extracellular pH (*4*). The ED-B–containing isoform of FN is immunohistochemically undetectable in normal adult tissue, with the exception of tissues undergoing physiologic remodeling (e.g., endometrium and ovary) and during wound healing (*4*). Furthermore, it has been demonstrated that ED-B is a marker of

Received Dec. 21, 2005; revision accepted Feb. 11, 2006.

For correspondence or reprints contact: Guus A.M.S. van Dongen, PhD, Department of Otolaryngology/Head and Neck Surgery, VU University Medical Center, De Boelelaan 1117, P.O. Box 7057, 1007 MB Amsterdam, The Netherlands.

E-mail: gams.vandongen@vumc.nl

tumor angiogenesis (*5*). ED-B is highly conserved in different species, having 100% homology in all mammalians thus far studied (human, rat, mouse).

Recently, a human recombinant scFv fragment directed against ED-B, designated L19, has been developed (*6*). Using its variable regions, several other L19 formats were constructed, including dimeric scFv ($(scFv)_2$), a human bivalent "small immunoprotein" (SIP), and a complete human IgG1 (*7*). Biodistribution studies with these constructs in tumor-bearing nude mice demonstrated selective tumor targeting, with the best performance of L19-SIP (*7*). L19-SIP also appeared to be the most favorable mAb format in preliminary radioimmunotherapy (RIT) studies, when labeled with ^{131}I (*8*). Additional animal studies with these mAb constructs confirmed the capacity of L19 for targeting of neovasculature and causing tumor infarction (*9,10*).

Radiolabeled L19-$(scFv)_2$ was also evaluated in clinical radioimmunoscintigraphy studies (*11*). The conjugate showed selective localization in tumor lesions in aggressive types of colorectal and lung cancer and appeared able to distinguish between quiescent and actively growing lesions. Also extensive immunohistochemical evaluation of ED-B expression in head and neck tissue biopsies has shown a relationship with aggressiveness (*12*).

Motivated by the promising results, we decided to explore L19-SIP also for RIT of squamous cell carcinoma of the head and neck (HNSCC). We had investigated the perspectives of RIT for treatment of HNSCC in the past because of the sensitivity of this tumor type for radiation. Using the radiolabeled mAb U36 or BIWA4, both directed against the target antigen CD44v6, promising antitumor effects had been observed in phase I dose-escalation RIT trials of patients with inoperable HNSCC (*13,14*). We hypothesized that ED-B might be even a better target for RIT of HNSCC. In comparison with CD44v6, which also shows high expression in some normal tissues such as skin and oral mucosa, ED-B expression seems much more restricted to tumors. In addition, it can be expected that the stromal target ED-B is better accessible for mAbs than the tumor cell target CD44v6, especially because of the compact structure of HNSCC.

As a future outlook for RIT of head and neck cancer, we previously proposed the combination with inhibitors of the epidermal growth factor receptor (EGFR). Indeed, the efficacy of RIT with radiolabeled mAb U36 in HNSCC xenograft–bearing nude mice was strongly enhanced when treatment was combined with an unlabeled anti-EGFR mAb (*15*). The rationale for such combination is (a) EGFR shows a high expression in 80%–100% of the head and neck tumors and plays a key role in their malignant behavior (*16,17*), (b) inhibition of EGFR results in radiosensitization (*18*), and (c) RIT and anti-EGFR therapy show complementary toxicity profiles. Because inhibition of EGFR was also shown to result in antiangiogenic effects such as decrease of VEGF synthesis (*19*), combining L19 RIT with anti-EGFR therapy might be particularly attractive.

In the present study, 2 HNSCC xenograft lines with representative ED-B expression were selected for tumor-targeting studies with radiolabeled L19-SIP. L19-SIP was radiolabeled with 2 candidate radionuclides for RIT, the residualizing radionuclide ^{177}Lu and the nonresidualizing radionuclide ^{131}I (for 1 experiment, ^{125}I was used as a substitute). The biodistribution of both conjugates was evaluated and compared in nude mice bearing the HNSCC xenograft lines. Finally, the therapeutic efficacy of RIT with ^{131}I-L19-SIP, either alone or in combination with the anti-EGFR mAb cetuximab, was evaluated in the same HNSCC xenograft lines.

MATERIALS AND METHODS

mAb, Xenograft Lines, and Radioactivity

Antibody L19-SIP (0.3–0.5 mg/mL), directed against the ED-B domain of FN, was obtained from the Institute of Pharmaceutical Sciences, Swiss Federal Institute of Technology, Zurich, Switzerland. Selection, construction, and production of L19-SIP (~80 kDa) have been described previously (*6,7*). A schematic drawing of its molecular structure was provided by Berndorff et al. (*8*). mAb cetuximab (C225/Erbitux; 2 mg/mL) was obtained from Merck. Cetuximab is a mouse–human chimeric anti-EGFR mAb that binds with high affinity to the receptor, blocks ligand-induced activation of receptor tyrosine kinase, and induces dimerization and downregulation of EGFR (*20*). The human HNSCC cell lines FaDu and HNX-OE have been described earlier (*21,22*). The HNX-OE line was developed at our own institute (*21*), whereas the FaDu line was obtained from Karl-Heinz Heider (Boehringer Ingelheim Austria).

^{131}I (7.4 GBq/mL) and ^{125}I (3.7 GBq/mL) were purchased from Amersham Biosciences, whereas ^{177}Lu (725 GBq/mg) was obtained from Perkin-Elmer.

Immunohistochemical Staining of HNSCC Xenografts

The 2 HNSCC xenograft lines FaDu and HNX-OE were characterized for ED-B and EGFR expression by performing immunohistochemistry with L19-SIP and cetuximab, respectively. Cryostat sections (5-μm thick) were air dried and fixed in cold acetone for 10 min at −20°C.

For immunohistochemical staining of ED-B, biotinylated L19-SIP was used in the first step, whereas the Dako ChemMate Detection Kit (streptavidin-alkaline phosphatase/red; DakoCytomation) was used for color development. In short, after fixation the sections were incubated in Tris buffer (50 mmol/L, pH 7.2) with 2% bovine serum albumin (BSA) for blocking for 30 min, followed by incubation with biotinylated antibody L19-SIP for 1 h at room temperature (RT). After extensive washing with the Tris buffer, sections were incubated with the ChemMate Detection Kit according to instructions provided by the supplier. After washing with demineralized water (demiwater), hematoxylin Gill III (Merck), 1:3 in water, was used as a counterstain followed by mounting in Kaisers glycerol gelatin (Merck).

For immunohistochemical staining of EGFR, cetuximab was used as the primary antibody followed by horseradish peroxidase (HRP)-labeled rabbit antihuman IgG (Dako). After fixation in 2% paraformaldehyde, sections were blocked with 2% BSA in phosphate-buffered saline (PBS) for 20 min at RT. Sections were incubated with cetuximab (10 μg/mL) for 1 h at RT. After extensive washing

with PBS, sections were incubated with rabbit antihuman IgG HRP (1:100) for 1 h at RT. After washing with PBS (3 times for 5 min), sections were incubated for 5 min with diaminobenzidine (1 mg/mL, 1:10) in PBS with 10 μL H_2O_2 for color development, followed by washing with demiwater and mounting in Kaiser's glycerol gelatin. Staining intensity was evaluated semiquantitatively.

Radiolabeling for Biodistribution Experiments

Preparation of ^{125}I-L19-SIP and ^{131}I-L19-SIP. Iodination of L19-SIP with either ^{125}I or ^{131}I was performed essentially as described previously (*23*). To a 20-mL β-scintillation glass vial coated with 75 μg IODO-GEN (1,3,4,6-tetrachloro-3α,6α-diphenyl-glycouril; Pierce Biotechnology), 50 μL Na_2HPO_4 (0.5 mol/L, pH 7.4), 72–150 μg L19-SIP in 450 μL Na_2HPO_4 (0.1 mol/L, pH 6.8), and 6.7–11.1 MBq ^{125}I or ^{131}I were added successively for a reaction of 4 min. Purification of radiolabeled L19-SIP was performed as described previously (*23*).

Preparation of ^{177}Lu-L19-SIP. Antibody L19-SIP was conjugated under strict metal-free conditions with *p*-isothiocyanatobenzyl-1,4,7,10-tetraazacyclododecane-1,4,7,10-tetraacetic acid (*p*-SCN-Bz-DOTA; Macrocyclics), essentially as described by Perk et al. (*24*). For conjugation, 125 μL *p*-SCN-Bz-DOTA (1.6 mg/mL in $NaHCO_3$, 0.1 mol/L; pH 9.0) and 875 μL (0.438 mg) of L19-SIP were incubated for 30 min at 37°C, pH 9.0. Approximately 1 *p*-SCN-Bz-DOTA moiety was coupled per L19-SIP molecule. L19-SIP-*p*-SCN-Bz-DOTA (150 μg) was labeled with ^{177}Lu (18.5 MBq) in a total volume of 700 μL CH_3COONH_4 (0.25 mol/L, pH 5.5). Purification of unlabeled and labeled L19-SIP-*p*-SCN-Bz-DOTA was performed as described previously (*24*).

Radiolabeling for Therapy Experiments

Preparation of ^{131}I-L19-SIP for therapy was performed according to the so-called "IODO-GEN–coated mAb method" essentially as described previously (*23*). Three milliliters L19-SIP (0.9–1.5 mg), 35 μL IODO-GEN/MeCN (1 mg/mL), and ^{131}I (884–1,880 MBq) were used for labeling. This method was recommended as it minimizes chemical and radiation damage to the mAb and allows the use of a large reaction volume (required because of the low concentration of L19-SIP available, 0.3–0.5 mg/mL).

Analysis

All conjugates were analyzed by instant thin-layer chromatography (ITLC) for radiochemical purity, by high-performance liquid chromatography (HPLC) and sodium dodecyl sulfate–polyacrylamide gel electrophoresis (SDS-PAGE) followed by phosphor imager analysis for integrity, and by an antigen-binding assay for immunoreactivity. ITLC analysis of radiolabeled L19-SIP was performed on silica gel–impregnated glass fiber sheets (Gelman Sciences). As the mobile phase, citrate buffer (20 mmol/L, pH 5.0) was used for ^{131}I- and ^{125}I-labeled antibody. ITLC samples of ^{177}Lu-labeled L19-SIP were first incubated for 5 min in a solution of ethylenediaminetetraacetic acid (50 mmol/L) and subsequently spotted on ITLC. As the mobile phase, 0.9% NaCl was used. HPLC analysis of radiolabeled L19-SIP was performed as described previously (*24*). The integrity of the radioimmunoconjugates was monitored by electrophoresis on a Phastgel System (Amersham Biosciences) using preformed high-density SDS-PAGE gels under nonreducing conditions and analyzed on a phosphor imager.

In vitro binding characteristics of radiolabeled L19-SIP were determined in an immunoreactivity assay essentially as described previously (*25*), using ED-B–coated Sepharose resin in PBS/1% BSA. Five serial dilutions, ranging from 100 to 6.2 μL resin per tube, were prepared in triplicate in PBS/1% BSA. L19-SIP (125 ng) labeled with ^{125}I, ^{131}I, or ^{177}Lu was added to the tubes and the samples were incubated overnight at 4°C for binding. Excess unlabeled L19-SIP antibody (10 μg per tube) was added to a second set of tubes with the lowest concentration of resin to determine nonspecific binding. Binding data were graphically analyzed in a modified Lineweaver–Burk plot, and the immunoreactive fraction was determined by linear extrapolation to conditions representing infinite antigen excess.

Biodistribution of L19-SIP

For the biodistribution experiments, female nude mice (Hsd athymic *nu/nu*, 25–32 g; Harlan CPB) bearing subcutaneously implanted HNSCC xenograft line FaDu or HNX-OE were used. All animal experiments were performed according to National Institutes of Health principles of laboratory animal care and Dutch national law ("Wet op de dierproeven", Stb 1985, 336).

Three biodistribution studies were performed. Biodistribution of coinjected ^{125}I-L19-SIP (0.37 MBq) and ^{177}Lu-L19-SIP (0.37 MBq) was assessed in FaDu-bearing nude mice ($n = 20$) in the first experiment. ^{125}I was used instead of ^{131}I to facilitate dual isotope counting with ^{177}Lu. Biodistribution of ^{131}I-L19-SIP (0.37 MBq) in FaDu- and HNX-OE–bearing nude mice ($n = 12$ each) was assessed in the second and third experiments, respectively. The tumor size at the start of the experiment was 83 ± 29, 73 ± 21, and 157 ± 95 mm^3 in experiments 1, 2, and 3, respectively. Mice received 10–16 μg L19-SIP in a total volume of 150 μL intravenously. At 3, 6, 24, 48, 72, and 144 h (experiment 1) or 24, 48, and 72 h (experiments 2 and 3) after injection, groups of 3 or 4 mice containing 5–8 tumors were anaesthetized, bled, killed, and dissected. Blood, tumor, and organs were weighed, and the amount of radioactivity was counted in a γ-well counter. In the case of ^{125}I and ^{177}Lu coinjection, dual isotope counting was performed. Radioactivity uptake was calculated as the percentage of the injected dose per gram of tissue (%ID/g), corrected for radioactive decay.

RIT with ^{131}I-L19-SIP

Three therapy experiments were performed using ^{131}I-L19-SIP. The first therapy study was designed to assess the maximum tolerated dose (MTD) in FaDu-bearing nude mice. The MTD, corresponding to the highest dose at which weight loss did not exceed 20%, was determined by monitoring the weight of FaDu-bearing nude mice injected intraperitoneally with diluent (0.9% NaCl) or increasing doses of ^{131}I-L19-SIP. Injection volume was too large to allow intravenous administration. Groups of 5 mice containing 8–10 tumors with a mean volume of 148 ± 61 mm^3 were treated with 37, 56, or 74 MBq ^{131}I-L19-SIP (134–146 μg). In the second and third experiments, FaDu- and HNX-OE–bearing nude mice were used, respectively, for studying the therapeutic efficacy of RIT alone and RIT in combination with cetuximab. Mice bearing 1 or 2 subcutaneous xenografts were treated at day 0 with a single intraperitoneal injection of ^{131}I-L19-SIP (74 MBq, 110 μg) or cetuximab (1 mg given 2 times a week intraperitoneally for 4 wk, as in our previous study on combined RIT with anti-EGFR therapy) (*15*), or a combination of both. The mean tumor volume at the start of the experiment was 143 ± 85 mm^3 (FaDu)

and 172 ± 101 mm^3 (HNX-OE). Treatment groups consisted of 8 mice with a total of 12–16 tumors (FaDu) and 13–15 tumors (HNX-OE) per group.

During treatment tumors were measured twice weekly for a planned period of 3 mo, and tumor volumes relative to the volume at the start of treatment were calculated. This period was extended for HNX-OE–bearing mice to 4 mo. Toxicity was monitored by measurement of body weight twice weekly. Mice were sacrificed when 1 of the tumors exceeded 1,000 mm^3. Average tumor volumes of the various groups were graphically depicted as long as at least 50% of the mice in a group were still alive.

An antitumor effect was also expressed as tumor growth delay. The tumor growth delay factor (GDF) was defined as the difference between the median values of the time required by tumors of treated and control animals to double their volume, divided by the median value of the time required by the tumors of the control mice to double their volume (*26*). Median instead of mean values were used because of the fact that sometimes tumors regressed completely. In addition, survival curves were constructed.

Statistical Analysis

Differences in tissue uptake between coinjected conjugates were statistically analyzed for each time point with Excel 2000 software (Microsoft) using the Student *t* test for paired data. Therapy experiments were analyzed using Excel 2000 software and SPSS 11.0 software (SPSS). Differences in average tumor volume between the various groups were statistically analyzed for each time point with the Student *t* test for unpaired data. Survival was calculated using Kaplan–Meier curves. Two-sided significance levels were calculated, and $P < 0.05$ was considered statistically significant.

RESULTS

Immunohistochemistry

The HNSCC xenograft lines FaDu and HNX-OE both expressed the ED-B domain of FN as well as EGFR. ED-B expression was highest in FaDu, whereas EGFR expression was similar for both lines (Fig. 1).

Radiolabeling

Labeling of L19-SIP with ^{125}I or ^{131}I for biodistribution and therapy experiments resulted in overall labeling yields of >70%. The radiochemical purity always exceeded 99%. Phosphor imager analysis of SDS-PAGE gels as well as HPLC analysis revealed optimal integrity of L19-SIP, irrespective of whether the mAb was labeled with a low or a high dose of ^{131}I. The immunoreactivity of iodinated L19-SIP was always >70% at the highest ED-B–resin concentration and >95% at infinite antigen excess. Labeling of L19-SIP–*p*-SCN-Bz-DOTA with ^{177}Lu resulted in an overall labeling yield of 66%, whereas the results of quality tests were comparable with those obtained using iodinated L19-SIP. The specific activities of the conjugates prepared for the biodistribution studies were 56–62 MBq/mg for iodinated L19-SIP and 73 MBq/mg for ^{177}Lu-L19-SIP. The specific activities for the therapy studies with ^{131}I-L19-SIP studies were 623–789 MBq/mg.

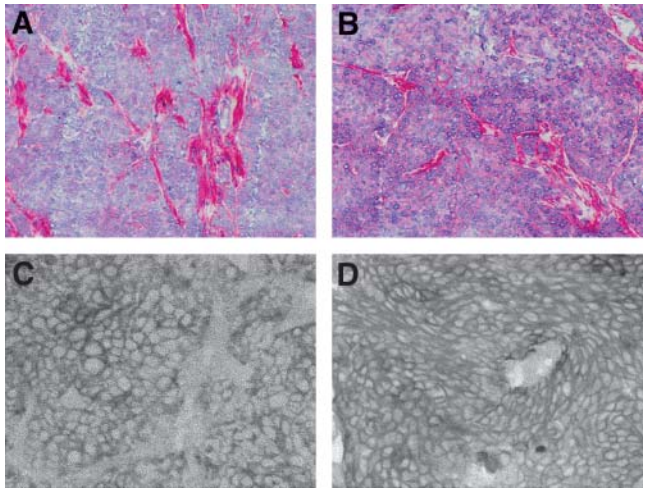

FIGURE 1. Immunohistochemical staining of HNSCC xenograft lines FaDu (A and C) and HNX-OE (B and D) with biotinylated L19-SIP (A and B) and cetuximab (C and D) for assessment of ED-B (red staining) and EGFR (staining of cell membrane) expression, respectively.

Biodistribution of L19-SIP

For comparison of the biodistribution of ^{125}I-L19-SIP (nonresidualizing radionuclide) with ^{177}Lu-L19-SIP (residualizing radionuclide) in tumor-bearing nude mice, both conjugates were coinjected. The average uptake in blood, tumor, and normal tissues is shown in Figure 2. Uptake of both radionuclides showed relatively small differences in blood, tumor, and most of the normal organs, such as tongue, sternum, heart, lung, bladder, muscle, colon, and ileum. Large differences, however, were observed in kidney, liver, and spleen, with much higher uptake of ^{177}Lu than of ^{125}I. On the basis of these results, we concluded that nonresidualizing radiolabels are better suited for RIT with L19-SIP than residualizing labels. Therefore, we decided to select ^{131}I for RIT experiments with FaDu- and HNX-OE–bearing nude mice. Before starting these experiments, tumor targeting with ^{131}I-L19-SIP was first compared in these 2 xenograft models. Uptake of ^{131}I-L19-SIP in FaDu tumors was higher than that in HNX-OE tumors, with uptake values at 24, 48, and 74 h after injection of 8.6 ± 1.6, 5.8 ± 0.4, and 3.4 ± 0.2 %ID/g, respectively, for FaDu and of 4.9 ± 1.1, 3.7 ± 0.7, and 2.5 ± 0.5 %ID/g, respectively, for HNX-OE (Figs. 3 and 4). Also tumor-to-nontumor ratios were in general higher for the FaDu xenograft line (Table 1). For example, although the tumor-to-blood ratios gradually increased for the FaDu xenograft line from 4.4 ± 1.8 at 24 h to 21.4 ± 1.7 at 72 h, for the HNX-OE xenograft line these values were 3.1 ± 1.2 and 15.1 ± 1.5, respectively.

Therapy of L19-SIP in FaDu- and HNX-OE–Bearing Nude Mice

The MTD was determined by monitoring the weight of FaDu-bearing nude mice injected with diluent or 37, 56, or 74 MBq of ^{131}I-L19-SIP. A dose-dependent weight loss was

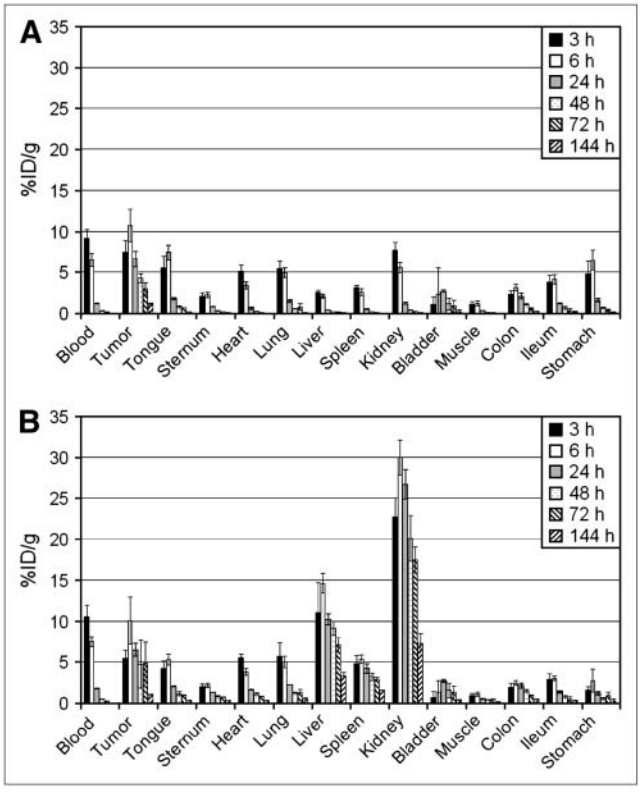

FIGURE 2. Biodistribution of intravenously coinjected ^{125}I-L19-SIP (A) and ^{177}Lu-L19-SIP (B) in FaDu xenograft–bearing nude mice at 3, 6, 24, 48, 72, and 144 h after injection.

observed and the MTD was established at 74 MBq (Fig. 5). At this dose level, weight recovered within 14 d, and no treatment-related deaths were observed.

The therapy experiments were set up to compare the efficacy of RIT with ^{131}I-L19-SIP in FaDu- and HNX-OE–bearing nude mice, either alone or in combination with twice-weekly injections of cetuximab for 4 wk.

FaDu tumors in the control group showed exponential growth with a mean tumor volume doubling time of 6 d

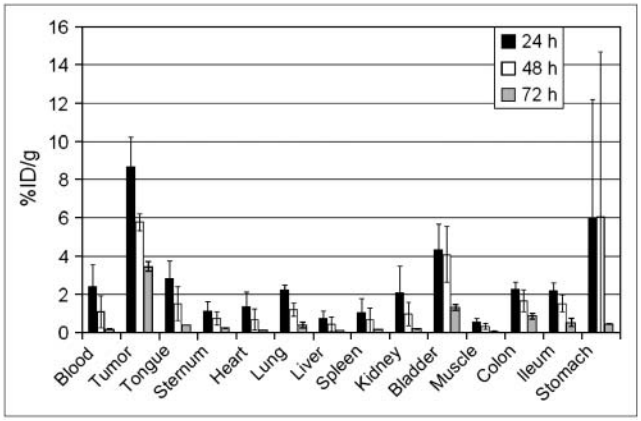

FIGURE 3. Biodistribution of intravenously injected ^{131}I-L19-SIP in FaDu xenograft–bearing nude mice at 24, 48, and 72 h after injection.

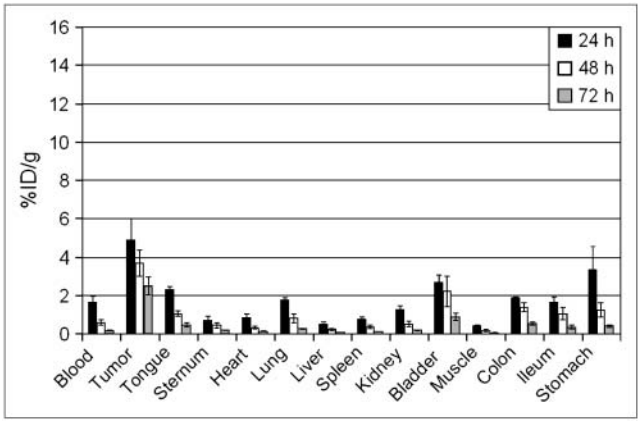

FIGURE 4. Biodistribution of intravenously injected ^{131}I-L19-SIP in HNX-OE xenograft–bearing nude mice at 24, 48, and 72 h after injection.

(Fig. 6A). Treatment with 74 MBq ^{131}I-L19-SIP caused a size reduction of all tumors, with a maximum decrease of average tumor volume to 74% ± 38% at day 18. At day 26, the tumors of this group had regrown to their initial volume. Thereafter, tumors grew more-or-less exponentially. The combination of RIT (74 MBq) with cetuximab showed an enhanced efficacy in comparison with RIT or cetuximab treatment alone, whereas toxicity was not increased (data not shown). Cetuximab treatment alone just slightly reduced the growth rate of FaDu tumors. When added to RIT, however, the size reduction started earlier (day 5) and the reduction was greater (50% ± 48% at day 26), whereas regrowth to the initial volume was later (day 35). The mean relative tumor volume in the RIT plus cetuximab treatment group was significantly smaller than that in the RIT alone group from day 4 to day 42. GDF values for the different treatment groups were as follows: RIT, 4.8; cetuximab, 0.2; and RIT plus cetuximab, 7.3. At the end of the observation period (day 90), 1 of 8 mice was still alive in the RIT group, whereas this value was 2 of 8 mice in the RIT plus cetuximab group (Fig. 6B).

RIT with a single injection of ^{131}I-L19-SIP was also evaluated in the second xenograft line HNX-OE (Fig. 7). The mean control tumor volume doubling time of this line was 8 d. In comparison with FaDu, the HNX-OE xenograft line was less sensitive for RIT (no reduction of the mean tumor size) and more sensitive for cetuximab treatment. Also, in this xenograft line, combined RIT plus cetuximab treatment showed the best therapeutic results without causing increased toxicity. Immediately after the start of combination treatment, the size of all tumors decreased, with a maximum decrease to 14% ± 10% at day 62, whereas at the end of the observation period just 3 of 14 tumors had a size larger than their initial volume. Consequently, all mice were still alive at day 90. In contrast, cetuximab treatment alone resulted just in a minor reduction of the mean tumor size for a short duration, whereas just 50% of the mice were still alive at day 90. GDF values for the different treatment

TABLE 1
Tumor-to-Tissue Ratios ± SD of Intravenously Injected ^{131}I-L19-SIP in FaDu and HNX-OE Xenograft–Bearing Nude Mice at 24, 48, and 72 Hours After Injection

Ratio	24 h		48 h		72 h	
	FaDu	HNX-OE	FaDu	HNX-OE	FaDu	HNX-OE
Tumor/blood	4.4 ± 1.8	3.1 ± 1.2	7.4 ± 3.7	6.3 ± 1.6	21.4 ± 1.7	15.1 ± 1.5
Tumor/tongue	3.4 ± 1.2	2.1 ± 0.6	4.7 ± 1.7	3.6 ± 1.1	9.3 ± 0.9	5.5 ± 1.6
Tumor/sternum	9.1 ± 3.7	8.2 ± 4.5	9.2 ± 3.2	8.3 ± 1.5	16.7 ± 1.3	14.1 ± 3.1
Tumor/heart	8.1 ± 3.6	6.0 ± 2.4	12.6 ± 6.7	11.5 ± 1.7	31.0 ± 3.2	22.7 ± 3.7
Tumor/lung	3.4 ± 1.7	2.8 ± 0.6	5.0 ± 1.3	4.7 ± 0.9	10.1 ± 3.5	9.9 ± 2.1
Tumor/liver	14.9 ± 6.8	10.7 ± 4.5	20.0 ± 10.3	18.1 ± 4.8	50.6 ± 5.6	38.4 ± 7.9
Tumor/spleen	11.3 ± 5.7	6.6 ± 2.0	14.2 ± 7.5	10.8 ± 1.8	31.4 ± 1.2	22.0 ± 5.1
Tumor/kidney	5.6 ± 2.7	3.9 ± 1.2	7.5 ± 2.9	7.2 ± 0.7	20.2 ± 3.3	14.2 ± 2.5
Tumor/bladder	2.3 ± 1.1	1.8 ± 0.2	1.6 ± 0.5	1.8 ± 0.5	2.8 ± 0.5	2.8 ± 0.5
Tumor/muscle	17.9 ± 6.4	11.9 ± 3.7	23.3 ± 9.7	22.4 ± 3.1	68.1 ± 15.5	47.5 ± 2.5
Tumor/colon	4.0 ± 0.9	2.6 ± 0.6	3.9 ± 1.2	2.7 ± 0.2	4.4 ± 0.9	4.6 ± 0.3
Tumor/ileum	4.2 ± 1.3	2.9 ± 0.6	4.1 ± 1.2	3.6 ± 0.4	8.5 ± 5.4	7.1 ± 1.8
Tumor/stomach	2.6 ± 1.5	1.7 ± 1.1	2.9 ± 2.2	3.1 ± 1.0	8.8 ± 1.8	6.3 ± 1.7

groups were as follows: RIT, 2.0; cetuximab, 8.5; and RIT plus cetuximab, 12.8.

Because not all tumors had regrown in the combination treatment group, the observation period was extended by 30 d. Survival after 120 d following injection was 3 of 8 for the group with cetuximab treatment alone and 5 of 8 for the RIT plus cetuximab treatment group.

DISCUSSION

In the present study, the potential of RIT with the anti–ED-B FN antibody L19-SIP was evaluated for treatment of HNSCC. To this end, nude mice bearing the HNSCC xenograft lines HNX-OE and FaDu were used as the model. Immunohistochemical evaluation of ED-B expression in these xenograft lines revealed a more intensive staining for the FaDu line than that for the HNX-OE line, whereas staining patterns were comparable with those previously observed for head and neck patient tumors in a study of Birchler et al. (*12*). They stained 53 malignant head and neck tumors, primary tumors as well as lymph node metastases, along with 8 benign tumors, 10 non-tumoral lesions, and 11 normal tissues. A strong positive

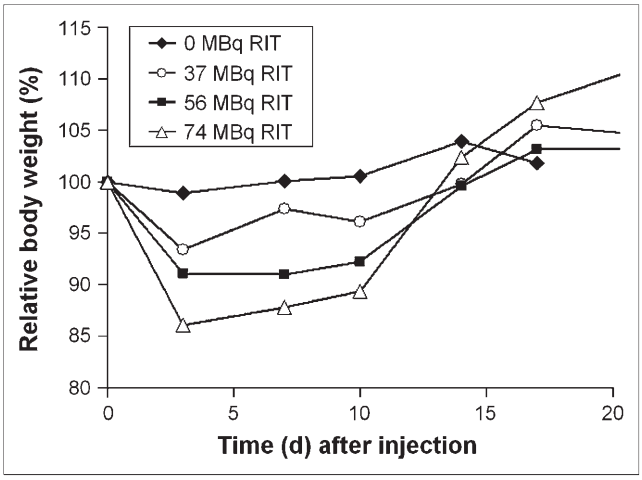

FIGURE 5. Mean body weights of FaDu xenograft–bearing nude mice intraperitoneally injected with diluent or increasing doses of ^{131}I-L19-SIP. Values are the mean of 5 mice. SDs have been omitted but were <5%.

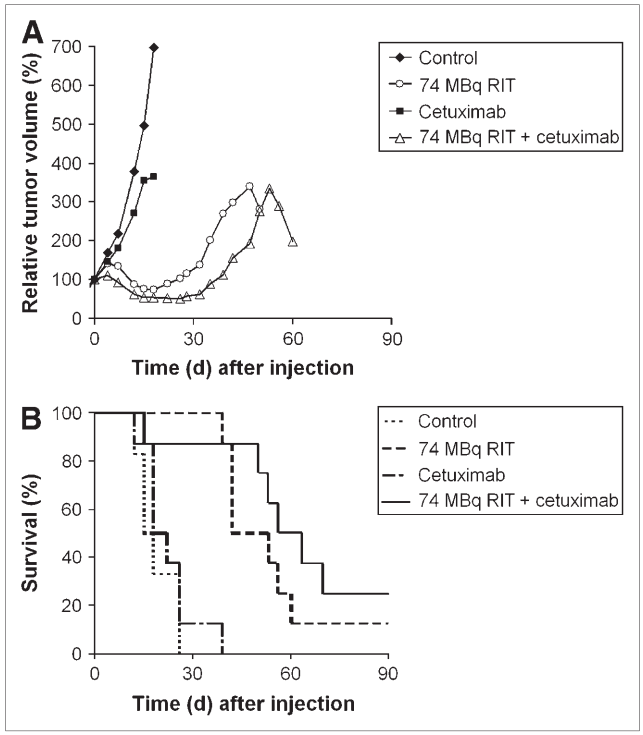

FIGURE 6. Mean tumor volume (A) and survival (B) of FaDu xenograft–bearing nude mice after intraperitoneal injection of ^{131}I-L19-SIP (RIT) at day 0, cetuximab (1 mg given 2 times a week intraperitoneally for 4 wk), or both. SDs have been omitted for sake of clarity.

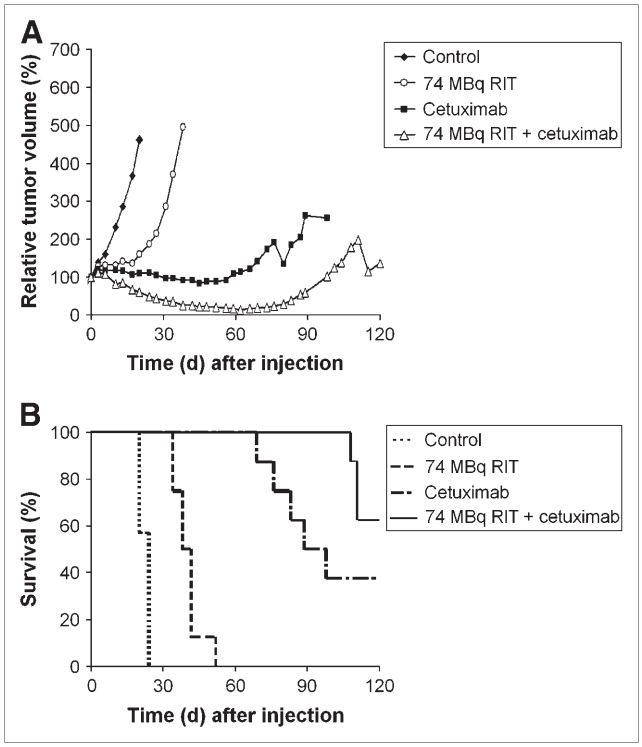

FIGURE 7. Mean tumor volume (A) and survival (B) of HNX-OE xenograft–bearing nude mice intraperitoneally injected with ^{131}I-L19-SIP (RIT), cetuximab (1 mg given 2 times a week intraperitoneally for 4 wk), or both. SDs have been omitted for sake of clarity.

staining was observed with L19 in 87% of the malignant tumors, with abundant expression around the neovasculature and in the stroma. Expression in benign tumors and nontumoral lesions was just 38% and 20%, respectively, whereas ED-B was totally absent in normal control tissue samples.

Two radionuclides were evaluated as candidates for RIT with L19-SIP, the nonresidualizing radionuclide ^{131}I and the residualizing radionuclide ^{177}Lu. If a mAb becomes internalized after binding to the tumor, the use of residualizing radionuclides for RIT might be advantageous because of higher tumor-to-nontumor ratios (*24*). No evidence was found, however, for such an advantage in the case of L19-SIP. The biodistribution of coinjected ^{125}I-L19-SIP (^{125}I as a substitute for ^{131}I to facilitate counting) and ^{177}Lu-L19-SIP in tumor-bearing nude mice showed just minor differences in uptake for tumor, blood, and most normal organs. In contrast, much higher uptake of ^{177}Lu than that of ^{125}I was found in organs of conjugate catabolism—kidney, liver, and spleen. On the basis of these results we decided to pursue using ^{131}I for RIT. Berndorff et al. (*8*) came to the same conclusion in an article that was published while our manuscript was in preparation. They compared the biodistribution of ^{125}I-L19-SIP and ^{111}In-L19-SIP in nude mice bearing mouse embryonal teratocarcinoma F9 tumors. Though tumor uptake was equal with both radionuclides, tumor-to-nontumor ratios were lower for the residualizing ^{111}In label. Dosimetric calculation using ^{125}I and ^{111}In as surrogates for the therapeutic radionuclides ^{131}I and ^{90}Y revealed the most favorable therapeutic index for ^{131}I-L19-SIP.

The MTD for single intraperitoneal administration of ^{131}I-L19-SIP was assessed at 74 MBq in FaDu-bearing mice. In our MTD study, weight loss was used as a gross toxicity criterion. Berndorff et al. (*8*) found the same MTD value for ^{131}I-L19-SIP, but they arrived at this value by a totally different approach. They performed dosimetric predictions using the biodistribution data of low-dose labeled ^{125}I-L19-SIP in F9-bearing nude mice. For dosimetry they had to make several assumptions—for example, (a) uniform distribution of radioactivity within the organs, (b) organ shapes as spheres, and (c) linear interpolation within the organs. The properness of MTD prediction, however, was confirmed by studying bone marrow toxicity after administration of 25–74 MBq ^{131}I-L19-SIP to nontumor-bearing nude mice. Berndorff et al. also found a high ^{131}I-L19-SIP uptake in uterus and ovaries (7.3 $\pm$ 1.8 and 3.1 $\pm$ 0.6 %ID/g at 24 h after injection, respectively; this was not determined in our study), which is consistent with known ED-B expression in these organs. Although they considered these reproductive organs not to be dose limiting, care should be taken when including fertile women in clinical RIT trials with ^{131}I-L19-SIP. For this purpose, performance of a scouting imaging procedure is recommended before ^{131}I-RIT to confirm tumor targeting and to estimate radiation dose delivery to both tumor and normal tissues. The use of ^{124}I-L19-SIP as the PET scouting agent in such approach might be particularly attractive (*27*).

RIT with ^{131}I-L19-SIP caused a significant tumor growth delay and improved survival in both HNSCC xenograft lines. However, no cures were observed. Antitumor effects were more pronounced for the FaDu line than for the HNX-OE line, which might be related to the higher ED-B expression in this xenograft line (Fig. 1) and the accompanying higher tumor uptake of L19-SIP as observed in biodistribution experiments (Figs. 3 and 4). Treatment of FaDu-bearing nude mice with 74 MBq ^{131}I-L19-SIP caused a size reduction of all tumors, whereas at day 26 the tumors had regrown to their initial volume. Antitumor effects in this human HNSCC xenograft line were more pronounced than those previously observed for mouse embryonal teratocarcinoma F9 xenografts (*8*). Although tumor uptake values of L19-SIP were almost twice as high in the F9 xenograft model as in the FaDu model (i.e., 17.5, 16.7, 15.3, and 12.0 %ID/g at 3, 6, 24, and 48 h after injection, respectively), tumor growth was delayed for just about 10 d. Because murine F9 teratocarcinoma is a very aggressive tumor, it might be that the potential of ^{131}I-L19-SIP became underestimated in these previous RIT studies.

Several options can be explored to optimize the efficacy of RIT with ^{131}I-L19-SIP, such as the application of RIT dose fractionation or repeated injections or the combination

with chemotherapy (*28–30*). Alternatively, RIT with ^{131}I-L19-SIP can be used in combination treatment enabling simultaneous targeting of multiple critical tumor pathways. In HNSCC, angiogenesis has been linked with tumor progression and worse outcome, and it might represent a resistance mechanism to anti-EGFR agents (*31,32*). In this context, it was interesting to combine ^{131}I-L19-SIP with cetuximab treatment. Cetuximab was a logical anti-EGFR candidate as this mAb had shown improved locoregional control and survival in combination with radiotherapy in a phase III study in locally advanced inoperable HNSCC (*33*). Our results showed an enhanced efficacy when RIT with ^{131}I-L19-SIP was combined with cetuximab treatment. Though the FaDu xenograft line was relatively sensitive for RIT and xenograft line HNX-OE was relatively sensitive for cetuximab, the best growth delay and survival rates were observed for both lines when treatment modalities were combined. Radiation response improvement by anti-EGFR treatment was also observed in previous RIT studies in HNSCC-bearing nude mice (*15*) as well as in clinical studies of external beam irradiation of head and neck cancer (*34*). An additional advantage for the combination with an anti-EGFR mAb, in comparison with other agents studied in combination with RIT, such as cytostatic drugs, is the low toxicity of anti-EGFR mAbs. In the present study, the combination of RIT with cetuximab treatment did not result in increased toxicity. Also, in patients, an increase of RIT-induced dose-limiting toxicity—which is mainly bone marrow toxicity—is not expected, in view of the fact that expression of EGFR is absent in the bone marrow.

CONCLUSION

RIT with ^{131}I-L19-SIP, a radioimmunoconjugate targeting the marker of tumor angiogenesis ED-B FN, caused a significant tumor growth delay and improved survival in nude mice bearing the HNSCC xenograft lines FaDu and HNX-OE. Antitumor effects were more pronounced for the FaDu line than for the HNX-OE line, which might be related to the higher ED-B expression in this xenograft line and the accompanying higher tumor uptake of L19-SIP as observed in biodistribution experiments. The efficacy of RIT was enhanced by combination with the anti-EGFR mAb cetuximab, without an increase in toxicity.

ACKNOWLEDGMENTS

This project is financially supported by the European Union FP6, LSHC-CT-2003-5032, STROMA. The publication reflects only the authors' view. The European Commission is not liable for any use that may be made of the information contained. The authors thank Dr. Gerard W.M. Visser, Dr. Lars R. Perk, and Maria J.W.D. Vosjan for their contribution to the experiments and Dr. Hartwig Kosmehl, Helios Klinikum Erfurt, Germany, for advise on immunohistochemistry.

REFERENCES

1. Brack SS, Dinkelborg LM, Neri D. Molecular targeting of angiogenesis for imaging and therapy. *Eur J Nucl Med Mol Imaging.* 2004;31:1327–1341.
2. Neri D, Bicknell R. Tumour vascular targeting. *Nat Rev Cancer.* 2005;5: 436–446.
3. Hurwitz H, Fehrenbacher L, Novotny W, et al. Bevacizumab plus irinotecan, fluorouracil, and leucovorin for metastatic colorectal cancer. *N Engl J Med.* 2004;350:2335–2342.
4. Carnemolla B, Balza E, Siri A, et al. A tumor-associated fibronectin isoform generated by alternative splicing of messenger RNA precursors. *J Cell Biol.* 1989;108:1139–1148.
5. Castellani P, Viale G, Dorcaratto A, et al. The fibronectin isoform containing the ED-B oncofetal domain: a marker of angiogenesis. *Int J Cancer.* 1994;59: 612–618.
6. Pini A, Viti F, Santucci A, et al. Design and use of a phage display library: human antibodies with subnanomolar affinity against a marker of angiogenesis eluted from two-dimensional gel. *J Biol Chem.* 1998;273:21769–21776.
7. Borsi L, Balza E, Bestagno M, et al. Selective targeting of tumoral vasculature: comparison of different formats of an antibody (L19) to the ED-B domain of fibronectin. *Int J Cancer.* 2002;102:75–85.
8. Berndorff D, Borkowski S, Sieger S, et al. Radioimmunotherapy of solid tumors by targeting extra domain B fibronectin: identification of the best-suited radioimmunoconjugate. *Clin Cancer Res.* 2005;11:7053s–7063s.
9. Birchler M, Viti F, Zardi L, Spiess B, Neri D. Selective targeting and photocoagulation of ocular angiogenesis mediated by a phage-derived human antibody fragment. *Nat Biotechnol.* 1999;17:984–988.
10. Nilsson F, Kosmehl H, Zardi L, Neri D. Targeted delivery of tissue factor to the ED-B domain of fibronectin, a marker of angiogenesis, mediates the infarction of solid tumors in mice. *Cancer Res.* 2001;61:711–716.
11. Santimaria M, Moscatelli G, Viale GL, et al. Immunoscintigraphic detection of the ED-B domain of fibronectin, a marker of angiogenesis, in patients with cancer. *Clin Cancer Res.* 2003;9:571–579.
12. Birchler MT, Milisavlijevic D, Pfaltz M, et al. Expression of the extra domain B of fibronectin, a marker of angiogenesis, in head and neck tumors. *Laryngoscope.* 2003;113:1231–1237.
13. Colnot DR, Quak JJ, Roos JC, et al. Phase I therapy study of ^{186}Re-labeled chimeric monoclonal antibody U36 in patients with squamous cell carcinoma of the head and neck. *J Nucl Med.* 2000;41:1999–2010.
14. Börjesson PKE, Postema EJ, Roos JC, et al. Phase I therapy study with ^{186}Re-labeled humanized monoclonal antibody BIWA 4 (bivatuzumab) in patients with head and neck squamous cell carcinoma. *Clin Cancer Res.* 2003;9: 3961s–3972s.
15. Van Gog FB, Brakenhoff RH, Stigter-Van Walsum M, Snow GB, Van Dongen GAMS. Perspectives of combined radioimmunotherapy and anti-EGFR antibody therapy for the treatment of residual head and neck cancer. *Int J Cancer.* 1998;77:13–18.
16. Grandis J, Tweardy D. Elevated levels of transforming growth factor alpha and epidermal growth factor receptor messenger RNA are early markers of carcinogenesis in head and neck cancer. *Cancer Res.* 1993;53:3579–3584.
17. Ang KK, Berkey BA, Tu X, et al. Impact of epidermal growth factor receptor expression on survival and pattern of relapse in patients with advanced stage head and neck carcinoma. *Cancer Res.* 2002;62:7350–7356.
18. Harari PM, Huang SM. Radiation response modification following molecular inhibition of epidermal growth factor receptor signaling. *Semin Radiat Oncol.* 2001;11:281–289.
19. Huang SM, Harari PM. Modulation of radiation response after epidermal growth factor blockade in squamous cell carcinomas: inhibition of damage repair, cell cycle kinetics, and tumor angiogenesis. *Clin Cancer Res.* 2000;6:2166–2174.
20. Mendelsohn J, Baselga J. Status of epidermal growth factor receptor antagonists in the biology and treatment of cancer. *J Clin Oncol.* 2003;21:2787–2799.
21. Hermsen MAJA, Joenje H, Arwert F, et al. Centromeric breakage as a major cause of cytogenetic abnormalities in oral squamous cell carcinoma. *Genes Chromosomes Cancer.* 1996;15:1–9.
22. Ranger SR. A new human cell line (FaDu) from a hypopharyngeal carcinoma. *Cancer.* 1972;29:117–121.
23. Visser GWM, Klok RP, Klein-Gebbink JW, Ter Linde T, Van Dongen GAMS, Molthoff CF. Optimal quality ^{131}I-monoclonal antibodies upon high-dose labeling in a large reaction volume and temporarily coating the antibody with IODO-GEN. *J Nucl Med.* 2001;42:509–519
24. Perk LR, Visser GWM, Vosjan MJWD, et al. ^{89}Zr as a PET surrogate radioisotope for scouting biodistribution of the therapeutic radiometals ^{90}Y and ^{177}Lu in tumor-bearing nude mice after coupling to the internalizing antibody cetuximab. *J Nucl Med.* 2005;46:1898–1906.

25. Birchler M, Neri G, Tardi L, Halin C, Viti F, Neri D. Infrared photodetection for the in vivo localization of phage-derived antibodies directed against angiogenic markers. *J Immunol Methods.* 1999;231:239–248.
26. Braakhuis BJM, Van Dongen GAMS, Vermorken JB, Snow GB. Preclinical in vivo activity of 2′,2′-difluorodeoxycytidine (Gemcitabine) against human head and neck cancer. *Cancer Res.* 1991;51:211–214.
27. Verel I, Visser GWM, Vosjan MJWD, Finn R, Boellaard R, Van Dongen GAMS. High-quality ^{124}I-labelled monoclonal antibodies for use as PET scouting agents prior to ^{131}I-radioimmunotherapy. *Eur J Nucl Med Mol Imaging.* 2004;31:1645–1652.
28. DeNardo GL, Schlom J, Buchsbaum DJ, et al. Rationales, evidence, and design considerations for fractionated radioimmunotherapy. *Cancer.* 2002;94:1332–1348.
29. Blumenthal RD, Alisauskas R, Juweid M, Sharkey RM, Goldenberg DM. Defining the optimal spacing between repeat radioantibody doses in experimental models. *Cancer.* 1997;80:2624–2635.
30. DeNardo SJ, Kukis DL, Kroger LA, et al. Synergy of Taxol and radioimmunotherapy with yttrium-90-labeled chimeric L6 antibody: efficacy and toxicity in breast cancer xenografts. *Proc Natl Acad Sci U S A.* 1997;94:4000–4004.
31. Caponigro F, Formato R, Caraglia M, Normanno N, Iaffaioli RV. Monoclonal antibodies targeting epidermal growth factor receptor and vascular endothelial growth factor with focus on head and neck tumors. *Curr Opin Oncol.* 2005;17:212–217.
32. Van Cruijsen H, Giaccone G, Hoekman K. Epidermal growth factor receptor and angiogenesis: opportunities for combined anticancer strategies. *Int J Cancer.* 2005;117:883–888.
33. Bonner JA, Harari PM, Giralt J, et al. Radiotherapy plus cetuximab for squamous-cell carcinoma of the head and neck. *N Engl J Med.* 2006;254:567–578.
34. Harari PM. Promising new advances in head and neck radiotherapy. *Ann Oncol.* 2005;16(suppl 6):vi13–vi19.